SDM 2013 Student Papers Competition

Shape Memory Alloy Rotor Blade Deicing

Florent Righi[1]
Texas A&M University, College Station, TX, 77843

Daniel B. Sullivan[2]
University of Maryland, College Park, MD, 20742

Darren J. Hartl[3]
Texas A&M University, College Station, TX, 77843

and

Jonathan Rogers[4]
Texas A&M University, College Station, TX, 77843

Because of power, space, and weight limitations, most modern rotorcraft lack deicing capabilities, thus reducing their operational capacity. The use of shape memory alloy (SMA) materials is an attractive solution for this problem due to their low weight and high deflection properties. This paper details a multi-stage feasibility study of a SMA-based rotor blade deicing concept. In the evaluated design, a thin aluminum sheet shaped as the leading edge of a NACA 0012 airfoil is connected to thin NiTi SMA wires. When the wires are actuated, they contract, deforming the aluminum sheet and fracturing the ice on its surface. First, the motivation for such a design is presented along with a brief overview of existing research into rotor blade deicing. The basic design is then described in more detail. The software analysis performed on the design is discussed. The design and construction of the prototype is also presented. When tested, the prototype successfully fractured a solid sheet of ice on its surface.

Sullivan, Righi, Rogers, Hartl, SMA Rotor Blade Deicer

Nomenclature

E	=	modulus of elasticity
E^M, E^A	=	modulus of elasticity of martensite, austenite
ν	=	poisson's ratio
ε	=	axial strain
α	=	coefficient of thermal expansion
ΔT	=	temperature gradient
M_s, M_f	=	martensite phase start and finish transformation temperatures
A_s, A_f	=	austenite phase start and finish transformation temperatures

[1] Masters Student, Department of Aerospace Engineering
[2] Undergraduate Summmer Research Grant Recipient, Department of Aerospace Engineering, Student Member
[3] Tees Research Assistant Professor, Department of Aerospace Engineering, Member
[4] Assistant Professor, Department of Aerospace Engineering, Member

C^M, C^A = martensite, austenite phase stress/temperature slope
H_{max} = maximum attainable transformation strain

I. Introduction

Icing is a dangerous condition experienced by a variety of aircraft, and currently there is no ideal deicing solution for helicopters. Icing is the process during which water in the atmosphere freezes on the surfaces of an aircraft, forming either rime ice, glaze (clear) ice, or a mixture of the two.[1] These ice deposits increase the weight of the aircraft and can alter its aerodynamic characteristics, increasing drag and reducing lift.[1] Collectively, these effects reduce the efficiency of the aircraft and place greater strain on the engine.[1] Analyzing icing of rotorcraft is significantly more complex than of fixed wing aircraft; unlike an aircraft wing, the airspeed along a rotor blade varies, the blades undergo rapid changes in angle of attack, and the blades are much thinner.[2] Asymmetrical ice deposits and asymmetrical shedding of ice can lead to dangerous vibrations consistent with unbalanced rotor blades.[2] Furthermore, a small amount of ice accumulation on the main rotor system can prevent helicopters from maintaining safe autorotational rpms.[2]

There are several existing deicing and anti-icing methods that have been developed for aircraft. A pneumatic boot system removes ice by inflating an air bladder beneath the surface of the aircraft, stressing and fracturing the ice.[3] An electro-thermal system uses electricity to heat up an area to either melt ice or prevent water from freezing.[3] Fluid ice protection systems combat ice formation by secreting a fluid over a surface that blends with atmospheric water to form a mixture with a lower freezing point.[3] Electro-impulse deicing systems function similarly to pneumatic boots; using variable electromagnetic fields, the system delivers a strong, rapid force to a surface, fracturing and delaminating ice.[3] Hot air systems typically use engine exhaust to warm critical surfaces of the aircraft.[3] Some of these systems are still in development for rotorcraft; currently, only thermal deicing systems have been approved for rotorcraft.[4] Such systems have high power requirements and can significantly increase the weight of the rotorcraft, leading many manufacturers to forgo the installation of any deicing or anti-icing capabilities.[4] This limits the operational capacity of these aircraft and poses a potential safety risk.

There is a need for a low-power, dependable deicing system. There are several potential solutions. Palacios, J. et al demonstrated a system that could remove ice from an aluminum plate using piezoelectric actuators to generate ultrasonic shear waves.[4] Another method involves applying a hydrophobic coating to rotor blades and other significant surfaces, but it is uncertain how such coatings would survive in the abrasive environment of a rotor blade. It is hoped that a design incorporating SMA actuators will meet these requirements.

The use of SMAs as smart structures in rotor blades is not a new concept. Rodin, Kondor, and Hanagud used SMA actuators to alter the camber of rotor blade in 1994.[5] Significant research has been done investigating the use of SMA actuators for inflight tracking of rotor blades.[6,7] These actuators are used to move small lift surfaces on rotor blades that allow for small corrections to be made to each blade's flight path. Researchers have also analyzed torsional SMA actuators for tilt rotor blades.[8,9,10,11] Gerardi, Ingram, and Catarella presented preliminary designs for a SMA-based deicing system in 1995.[12,13] Their designs called for the leading edge of an airfoil to be covered with an SMA sheet, the actuation of which would delaminate ice deposits.

The transformation achieved with an SMA actuator is a result of internal phase transformations. There are two phases, the martensite phase and the austenite phase. At lower temperatures, the material is in the martensite phase and has a low apparent yield stress and low modulus of elasticity.[14] When the temperature of the material is increased, it transitions from the martensite phase to the austenite phase.[14] During this process, the SMA can recover its original shape and become more rigid. This recovery is known as the shape memory effect (SME).[14] This transformation to austenite, sometimes called the reverse transformation, begins when the A_s temperature is reached and proceeds until the A_f temperature

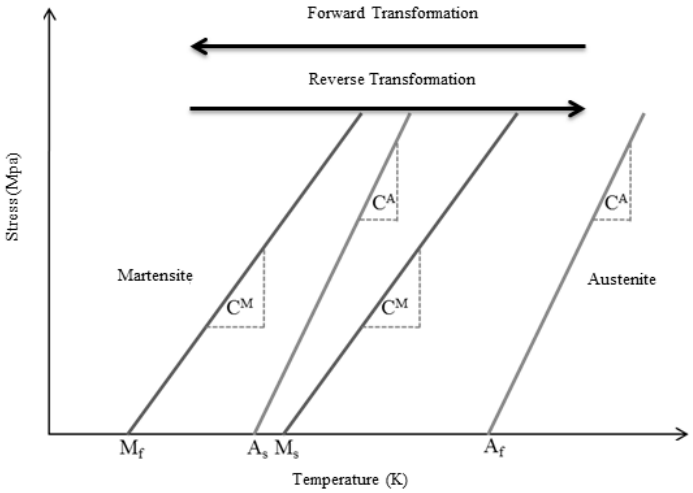

Figure 1. SMA stress vs. transformation temperature plot

is achieved. At or above A_f, the entirety of the SMA consists of the austenite structure and the SME is complete. When the temperature of the SMA is decreased, the material structure changes from austenite to martensite, known as the forward transformation. These changes begin and end at M_s and M_f, respectively. The values of these temperatures vary approximately linearly with the effective stress in the SMA, and the slopes of the linear relationships are characterized by C^M and C^A. In most SMA material systems, including that studied herein, a restoring force is required to restore the SMA back to the shape it possessed prior to the reverse transformation.

This paper outlines a feasibility study of a SMA-based rotor blade deicer design. Shape memory alloys show promise in providing a low power, high force mechanism for deicing. In the design proposed here, a thin aluminum sheet shaped as the leading edge of a NACA 0012 airfoil is connected to thin NiTi SMA wires. When the wires are actuated, they contract, deforming the aluminum sheet and fracturing the ice on its surface. The paper begins with a more detailed description of the evaluated design. Then the software analysis of the design is presented. The design, construction, and testing of the prototype is then described. Finally, the results of the testing are presented and discussed.

II. Preliminary Design

The feasibility study outlined here followed a model-based design process in which FEA and CAD software tools were used to extensively for design optimization well before any actual hardware was constructed. This ensured maximum performance of the design at minimal prototyping costs. When a prototype was finally constructed, performance matched FEA predictions almost exactly. The fidelity and efficiency of this predictive process, in which design refinements were made through software tools only and the hardware product matched performance predictions precisely, was instructive in and of itself.

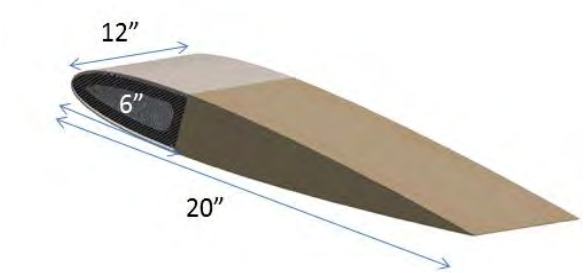

Figure 2a. Basic Design Dimensions

Figure 2b. Basic Design Dimensions

Before beginning the software analysis and prototype design, the basic design concept was first established. The basic concept was designed to be simple yet easily recognizable by the helicopter industry. The design mimicked the dimensions and shape of the rotor blade of a Bell UH-1 model helicopter and used a NACA 0012 airfoil. The chord length of the design was 20”, similar to the 19” length found on the UH-1. This design was established under the requirements that it be easily constructible and fairly low in cost. The budget for this prototype was restricted to $1000.

As illustrated in Fig. 2b, the design was made of four components, the D section, the aluminum sheet, the SMA actuators, and the fairing.

The D section, number 1 in Fig. 2b, is the section of the airfoil from the leading edge to the position of max height at 30% chord length. A hollow D section was used to reduce material.

The aluminum sheet, number 2, is ideally formed into a NACA 0012 airfoil shape around the D section and attached at the leading edge. This is the component that is actuated by the SMAs. When the SMAs are activated, the aluminum sheet is deformed, stressing and fracturing any ice deposited on its surface. The elastic nature of the aluminum sheet also provides the restoring force to re-strain the SMA wires. This aluminum sheet mimics the abrasion strip found on real helicopter blades.

The SMA actuators, number 3, are located between the D section and the aluminum sheet. Flexinol SMA wires were chosen as the actuators for reasons of cost and availability. These wires are attached to the rear of the aluminum sheet. At room temperature, the wires are in the martensite phase and are pre-strained 4%. When actuated, the wires contract via the SME, pulling the rear of the aluminum sheet forward. Because the aluminum is secured to the D section at the leading edge, the aluminum is deformed during this process. When the forward transformation begins, the elastic nature of the aluminum sheet is used to re-strain the wires to their original pre-strained length. In other words, the aluminum sheet acts as a spring and provides the necessary restoring force to the SMA.

The fairing, number 4, is the final component in the basic design. The only purpose of the fairing is to complete the aerodynamic shape of the rotor section. This property was only significant for evaluation of the prototype in a wind tunnel. Thus, it was not modeled in the simulations.

III. Software Analysis

The Abaqus program was used to perform FEA on the basic design. Parts were simplified but not beyond the constraints of the study. The aim of the analysis was to predict the behavior of the system and to provide a vote of confidence for the feasibility of the prototype design. This analysis was also used determine design parameters for the prototype such as the SMA wire diameter, number of SMA wires, and the aluminum sheet thickness. The software analysis was conducted in three different stages.

A. 3D Beam Elements: Approximate SMA Model

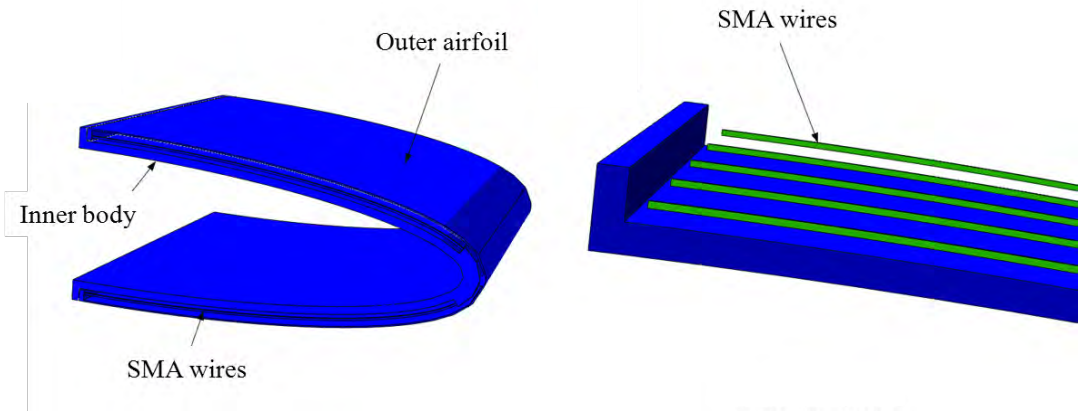

Figure 3. 3-D Beam Element SMA Approximation Simulation

The behavior of SMAs can be challenging to analyze. To gain a better understanding of the process, the first FEA simulation mimicked the behavior of the SMA wires with a simpler model. As shown in Fig. 3, the assembly was simple and only used three different parts: a solid inner body, a solid outer airfoil, and 3-D beam elements representing the SMA wires. The inner body was considered as a non-deformable body while the outer airfoil had the material properties of aluminum, an elastic modulus E of 70,000 MPa and a Poisson's ratio v of 0.33.

The recoverable strain of the SMA was set to 5%, a reasonable assumption based on information from the manufacturers of the Flexinol wires utilized in this study. In the most simplistic sense, the same memory behavior can be modeled using an artificial thermal expansion, though such modeling neglects the stress-temperature coupling shown in Figure 1, as well as a host of other effects. In this way, the 1-D behavior of the SMA can be approximated by equation 1:

$$\varepsilon = \alpha \Delta T \tag{1}$$

Thus, any artificial combination of the thermal coefficient and the temperature change resulting in a total strain change of 5% is applicable. In this instance, a very high thermal expansion coefficient (5%) and a minimal temperature change (1K) were used. This approximation provided an early visualization of the design actuating and returning to its original state. This success allowed the analysis of the design to progress to the next level.

B. 3-D Beam Elements: Accurate SMA Model

An improved analysis was implemented using a user material subroutine, which is an implementation of an accurate 3-D SMA constitutive model that also considers pre-strain in an SMA body, as existed in the wires employed. The UMAT allows physically realistic SMA properties to be used in the simulation. These material properties are listed in Table 1.[15]

Table 1. UMAT SMA Material Properties

Property	Value	Units
M_s	289	K
M_f	263	K
A_s	308	K
A_f	335	K
C^M	6,000	MPa/K
C^A	7,000	MPa/K
E^M	7.00E+7	MPa
E^A	7.00E+7	MPa
ν (Martensite & Austenite)	0.33	-
α (Martensite & Austenite)	0	-
H_{max}	0.049	-

This higher fidelity analysis provided a more accurate visualization of the design concept. A critical aspect of the analysis was the determination of the axial stress present in the SMA during after the course of the actuation process. Recall that the different transformation temperatures (M_s, M_f, A_s, A_f) vary approximately linearly with axial stress. Thus a smaller SMA cross sectional area results in higher stress and therefore higher A_s and A_f temperatures. This strong relationship between wire size and actuation completion temperature then required that the stress levels in the SMA be monitored and adjusted via adjustment of the aluminum shell configuration or a change in wire diameter.

C. 1-D Truss Elements: Accurate SMA Model

A second analysis replaced the 3-D beam elements with 1-D truss elements. A graph and table describing the transformation process of the SMA wires in more detail are provided in appendix entry A-1. The remainder of the simulated model was altered to incorporate the prototype materials and dimensions at this stage of the design process. These properties are supplied in Table 2.

Table 2. Final Simulation Assembly Component Properties

Function	Material	Thickness (mm/in)	*E* (MPa)
Aluminum Sheet	Aluminum	0.8128/0.032	72,000
D section	ABS Plastic	12.7/0.5	2,700

One of the main constraints of this simulation was the maximum stress in the wires. It was estimated that permanent damage could occur to the wires at a stress of roughly 300 MPa. Accordingly, several assembly configurations featuring different numbers of wires were simulated and the results are displayed in Table 3.

Table 3. Wire Stress Study

Property	4 Wires	6 Wires	8 Wires
Wire cross sectional area (mm^2)	0.033	0.028	0.020
Wire diameter (mm)	0.20	0.18	0.16
Max Von Mises stress, 375K (MPa)	448	352	265
Distance not recovered in forward transformation	10%	16%	30%

As expected, adding wires reduced the stress in each wire. However, as the sum of the cross sectional areas of the individual wires increased, the effectiveness of the aluminum sheet in re-straining the wires decreased, and two-way actuation would become impossible. Thus, as the number of wires in the assembly increased, the wire diameter needed to be decreased. While decreasing the wire diameter increases the stress experienced by each wire,

increasing the number of wires in the configuration results in a net reduction of stress. The 8 wire configuration has appealing wire stress levels, but the recovery performance is disappointing. Compromising between stress and recovery characteristics, the higher-stress 4 and 6 wire configurations were deemed more favorable for the prototype.

IV. Prototype Design and Construction

The prototype was designed and constructed for evaluation and demonstration of the design concept. More specifically, there were four goals associated with the prototype:

i. Deformation of the aluminum sheet with SMA actuation
ii. Restoration of the system to its original state following actuation
iii. Fracturing of ice on the aluminum sheet during actuation
iv. Delamination of ice from the aluminum sheet during actuation in the presence of an airstream

The design and construction of the prototype was a significant portion of this project. They are most easily discussed in terms of the individual components: the D section, the aluminum sheet, the SMA wires, the fairing, and the ice deposition box.

A. D Section

While the basic design of the D section is fairly simple, it required more design effort compared to any other component. The main reason for this is that the D section is the base of the design; every other component connects to it and depends on it.

The decision was made early on to construct the part with a rapid prototyping process. This involved designing the part in 3D CAD software, SolidWorks, and then fabricating the part out of ABS plastic with a 3D printer. This method allowed for a more complex design to be fabricated very accurately and in a short amount of time.

The final CAD model of the D section is presented in Fig. 5, and the assembled component is shown in Fig. 6. Circle 1 indicates the split state of the part. This feature resulted from uncertainty surrounding the attachment of the SMA wires to the aluminum sheet. Without this split, it would be extremely difficult to access attachment points located between the aluminum sheet and the D section after the aluminum was bolted onto the D section. To assist in the proper alignment of the two parts of the D section, guidance tabs were added. They can be seen jutting out of the rear component, and the corresponding cavities can be seen in the front component.

Circles 2-4b concern various attachment points and methods. Circle 2 indicates bolt access holes. These spaces allowed access to the bolts used to fasten the aluminum sheet to the D section at the leading edge. Circle 3 marks two adjacent screw holes in the rear component that were used for attaching the D section to the fairing. Two matching holes can be seen on the far side of the rear component. Circles 4a and 4b designate bolt tabs and bolt holes used to secure the two

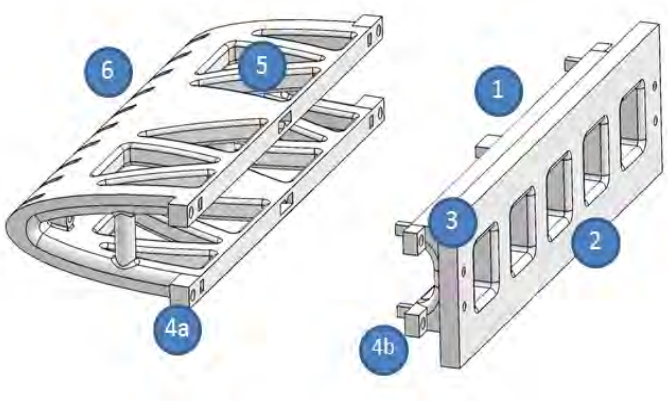

Figure 5. D section CAD model

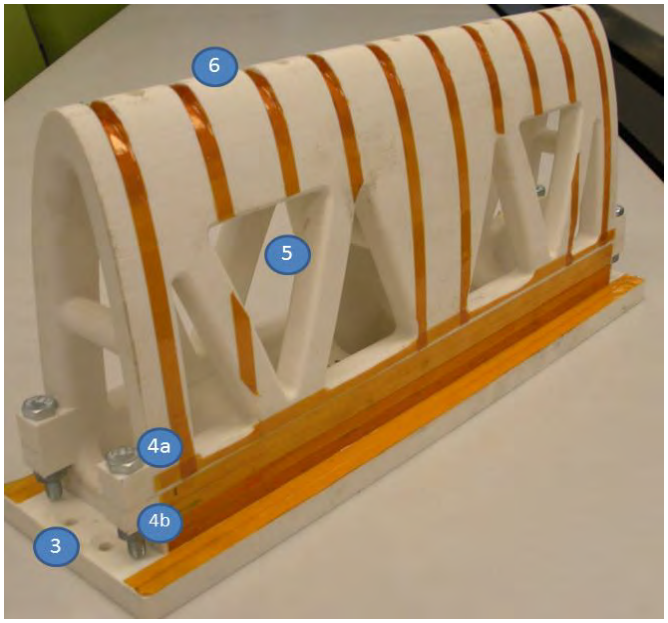

Figure 6. Assembled D section

components of the D section to each other.

Circle 5 draws attention to the triangle cut outs in the D section wall. These cutouts served to reduce the amount of material used in fabricating the part. Besides reducing the cost and weight of the piece, the cutouts also reduced the part's fabrication time.

Lastly, circle 6 marks ten notches evenly spaced on the leading edge of the part. The notches served as paths for the SMA wires to travel around the D section. The notches allowed for the wires to be easily aligned. This design also allowed for the longest possible SMA wire to be used; the wires have a fixed strain, so the longer the wire is along the chord of the rotor section, the greater the displacement of the wire and the greater the deflection of the aluminum sheet. Ten notches were incorporated to allow for extra wires.

While ABS plastic is a very robust material, there was a potential melting problem in the design. ABS plastic begins to melt at 105°C, and the SMA wires can reach higher temperatures during actuation. To avoid melting the ABS, Kapton tape, a high temperature adhesive, was installed on all sections of the D section that had a chance of touching the SMA. The tape is the orange material in Fig. 6.

The fabrication of the D section was quick thanks to the 3D printing process. The part was printed in 30 hours and required a 20 hour acid bath to dissolve support material. An image of the part mid-printing is displayed in appendix entry A-2.

B. Aluminum Sheet

The second important component of the design is the aluminum sheet. The most challenging part of designing and constructing this component was determining which aluminum alloy would best suit the application. The sheet had to possess enough springiness to re-strain the SMA wires following actuation, but it also had to be weak enough to be deformed by the wires. Several different thickness and types of aluminum were evaluated before 0.020" thick sheet of 3003 aluminum was chosen. Fig. 7 depicts the final CAD model of the aluminum sheet. The top and bottom of the sheet are symmetric. Fig. 8 shows the actual aluminum sheet.

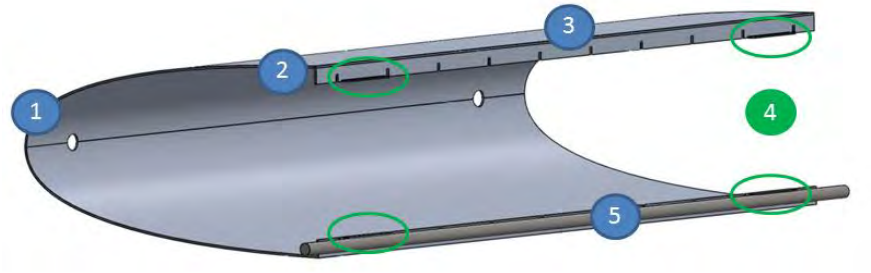

Figure 7. Aluminum sheet CAD model

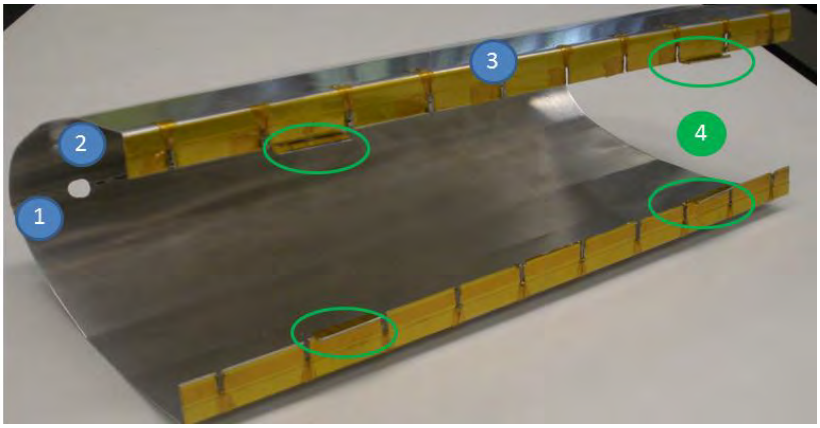

Figure 8. Assembled aluminum sheet

Circle 1 indicates one of the two bolt holes for attaching the sheet to the D section. The first manufactured sheet had five bolt holes, but experimentation showed that two bolts were sufficient. The elimination of the center bolt holes provides a smooth surface for ice to form.

The next challenging aspect of the aluminum sheet design was attaching the SMA wires. After much experimentation, it was determined that the best method was to attach each wire to a threaded rod and to hold the threaded rod to the aluminum with tension alone. Circle 2 marks a fold in the aluminum sheet. The threaded rod sits behind this fold and pushes on the fold when the SMA wires contract. Circle 3 indicates ten slits cut in the upper flap. These slits are aligned with the notches in the front of the D section and allow the SMA wire to pass through the aluminum to the threaded rod. Marked with green ovals, short flat tabs jut out from the flaps. These tabs prevent the threaded rod from slipping off the aluminum sheet. Circle 5 marks a threaded rod in its proper position; an identical rod was positioned along the upper flap.

Another advantage of aluminum 3003 is that it is easily shaped. The airfoil-like shape was achieved by making multiple bends in a flat sheet with a sheet metal brake. The metal tabs were later epoxied onto the aluminum sheet. Kapton tape was also added to the slits to prevent electrical contact between the circuit and the aluminum sheet.

C. SMA Wires

Flexinol SMA wires were used in the prototype. Using results from the software analysis of the design, 0.008" (0.2 mm) diameter wire was chosen. The wire arrived prestrained, eliminating the need for SMA training. Fig. 9 depicts the wire attachment method. The wire, circle 1, was crimped in a ring terminal, circle 2, which was then placed on the threaded rod. Because the wire was very thin, it had to pass through the crimp twice to be secured.

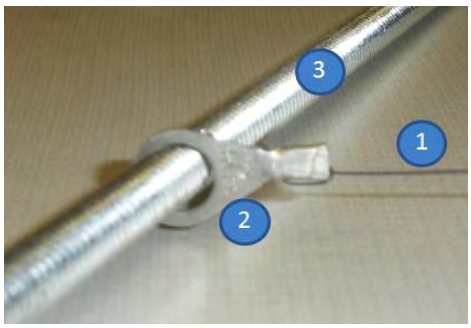

Figure 9. SMA wire attachment method

A procedure was followed to ensure that each wire was of equal length; any slack in a wire reduced or eliminated the effectiveness of that actuator. First, the aluminum sheet was formed and placed on the D section. Second, a preliminary wire was sized to this setup. Third, all the following wires for that configuration were constructed on a jig board, essentially two nails poking through a board that were placed using the preliminary wire. An image of this jig board is available in appendix entry A-3.

The wires were most easily actuated with resistive heating. In this process, the temperature of a resistor, in this case a certain length of SMA wire, is increased with an electrical current. The wires were set up in a parallel circuit with the ring terminal serving as a mechanical and an electrical connection. The threaded rod was used as the connection between the individual wires. The expected length of each SMA wire was obtained from the CAD models of the prototype and was used to calculate each wire's resistance. Recommended current values were provided by the wire manufacturers. The software analysis provided the number of wires expected in the design, allowing the max expected current to be estimated. The electrical demand was small enough to be met by a lithium polymer battery.

D. Ice Deposition Box

One of the challenges that was encountered early in the design process was freezing ice on a curved aluminum sheet. To counter this challenge, a mold was designed that would hold the assembled prototype in place and allow for water to be poured in a thin layer around the aluminum sheet. The entire assembly would then be placed in a freezer. The mold was constructed by pouring expanding, closed cell foam in a five sided box around the prototype. The prototype was protected by a layer of wax paper. In addition, several layers of paper were placed on the aluminum sheet underneath the wax paper to displace the foam and provide space for water in the final mold. A CAD model of the box as well as the complete box can be seen in appendix entry A-4. The effectiveness of the box is currently being evaluated.

E. Assembly Views

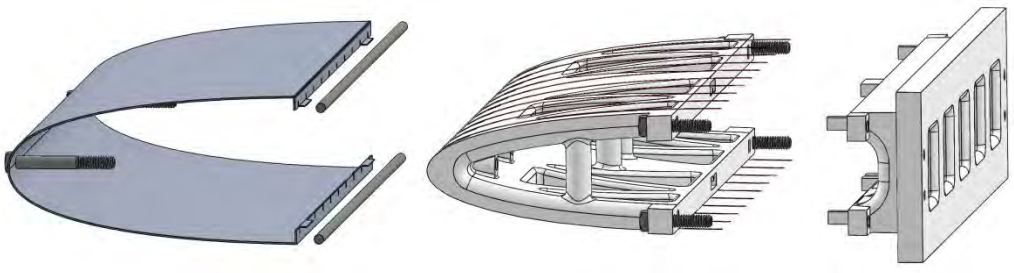

Figure 10. Prototype Assembly: CAD Exploded View

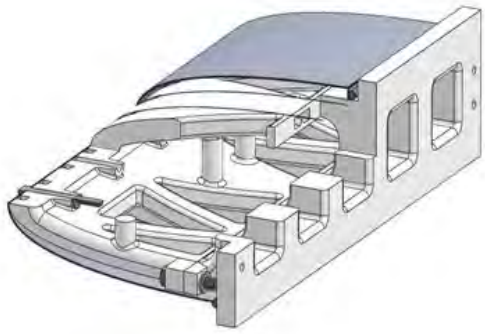

Figure 11a. Prototype Assembly CAD Model

Figure 11b. Prototype Assembly

Results

The prototype was successfully actuated. Two different wiring harnesses and three different aluminum sheets have been used, both with four and six wires. The first aluminum sheet was the 3003 alloy, the second was a slightly thicker and stronger 6061 alloy, and the third was a 3003 sheet fitting the description in the prototype section above. Although no data was collected for the first two configurations, qualitative observations determined that the 3003 sheet deformed more than the 6061 sheet. This encouraged the construction of the second 3003 sheet and harness. The sheet and wiring harness were better constructed than the first set. The wires were also slightly longer, allowing for small improvement in deformation. A brief amount of data has been collected for this most recent aluminum sheet and wiring harness and is presented in Table 4. More testing is planned for the near future, including deflection testing for multiple wires, ice testing, and possibly wind tunnel testing.

Table 4. Experimental Deflection Results

4 Wires	Test 1	Test 2	Test 3
Chordwise Displacement (in)	0.084	0.098	.099

V. Discussion

There is limited data to analyze, but it has implications for future testing. The wires in the final wire harness were 11.25 inches long. Because they loop around the entire D section, one wire can be analyzed as two separate wires traveling from the threaded rod to the leading edge of the D section. The length of one of these wires is roughly 5.6”. Calculating for a 4% strain, one would expect the chordwise deflection of the aluminum to be around 0.23”. However, the observed deformation is not even half of that value.

One factor that contributes to this difference is that the path of the wire along the D section is not flat. Thus using the length of the wire to calculate the expected strain will produce a value slightly higher than what is actually obtainable. Another factor that requires further investigation is the number of wires. Four wires may be too few to fully deform the aluminum. Recall that as the stress in the wires increases, so do the transformation temperatures. It is possible that the wires are under enough stress that the wire is no longer fully transforming to the austenite phase. This can be tested by adding more wires to the wire harness.

Brief calculations show that the prototype, operating at 5.4 Volts and sourcing 2.6 Amps, requires 14 Watts of electrical power for a 1 foot rotor section span. If this system were to be applied to the entire 48 feet of the Bell UH-1 model 205’s two blade rotor disk diameter, the system would require a total of 675 Watts. However, because significant testing is still required and because no ice has yet been broken by the prototype, nothing can definitely be determined yet by comparing the electrical demands of the prototype to existing deicing methods.

VI. Conclusion

This paper presented a feasibility study focused on a SMA based rotor blade deicing concept. The rotorcraft industry is interested in a more efficient and reliable deicing system to increase the safety and expand the operating conditions of aircraft. Shape memory alloys show potential in providing a low power, high deflection deicing mechanism. This study began by describing the general design concept that was evaluated, and then presented the

software analysis performed during the design, as well as detailed the design, construction, and testing of a prototype. Current results show that the concept is promising and justifies further research in SMA-enabled deicing.

Appendix

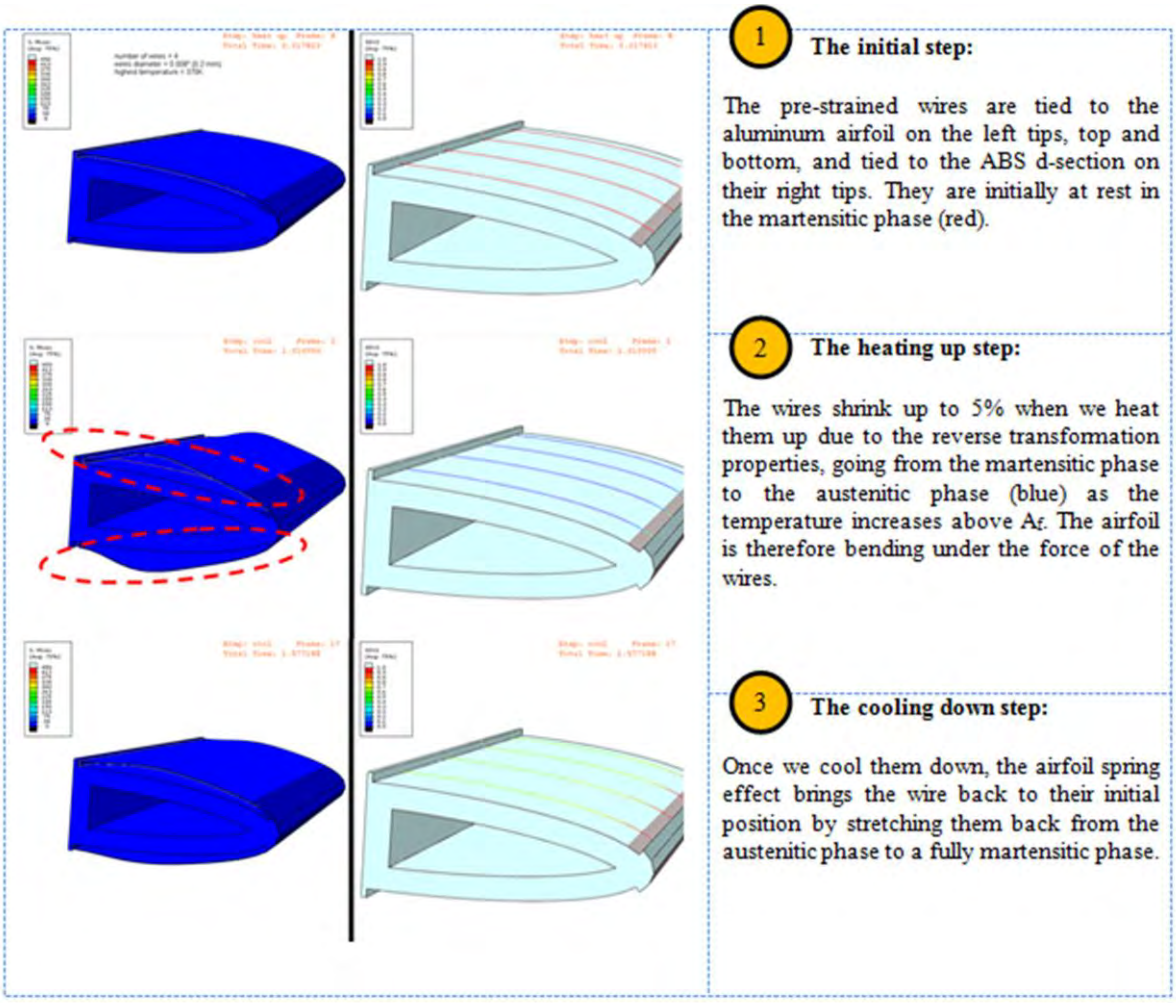

A-1. Transformation Path of SMA Wires in Software Analysis

A-2. 3D printing of D section in progress

A-3. Jig board used for constructing wires

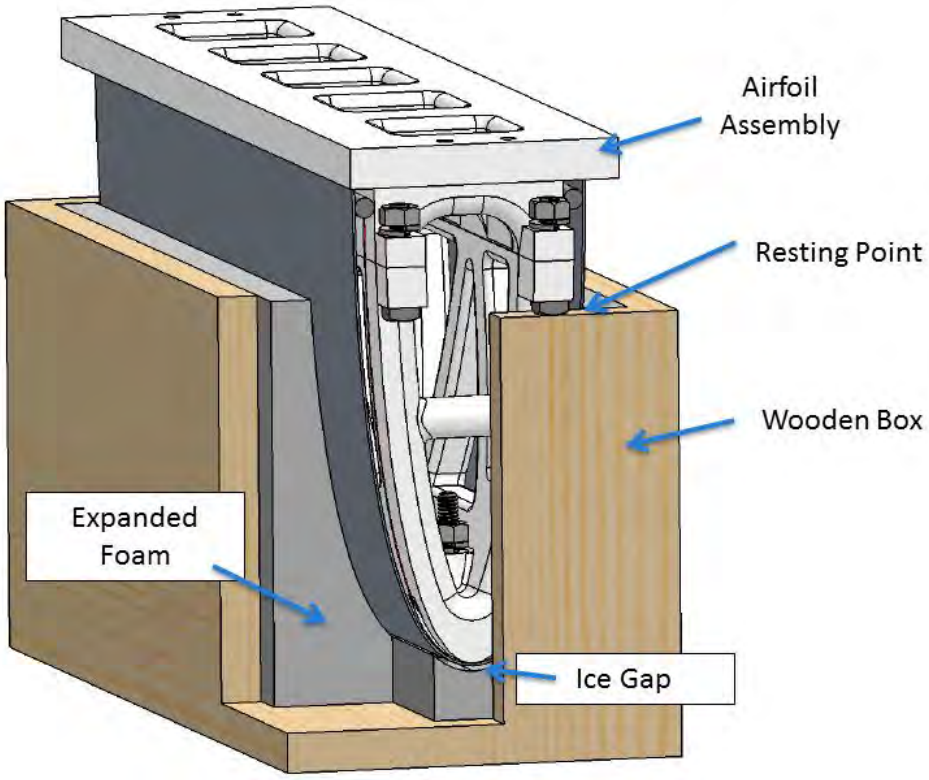

A-4. Ice Box Assembly CAD Model

Acknowledgments

F. Righi and D. Sullivan thank Robert Long for his contributions and help with electronics. They thank Rodney Inmon for his advice and guidance. D. Sullivan would like to thank the Department of Aerospace Engineering at Texas A&M University for their support under the Undergraduate Summer Research Grant program (NSF Award #1005178). F. Righi thanks the International Institute for Multi-Functional Materials for Energy Conversion (IIMMEC) (NSF Award #0844082) for providing funding for his time at Texas A&M University.

References

[1]Heinrich, A, Ross, R., Zumwalt, G., Provorse, J., Padmanbhan, V., Thompson, J., and Riley, J., The U.S. Department of Transportation and the FAA, "Aircraft Icing Handbook," Vol. 1, March 1991.

[2]Flight Safety Foundation, "Inflight Icing and the Helicopter," *Helicopter Safety*, Vol. 16, No. 6, Nov./Dec. 1990, pp. 1-4

[3]Heinrich, A, Ross, R., Zumwalt, G., Provorse, J., Padmanbhan, V., Thompson, J., and Riley, J., The U.S. Department of Transportation and the FAA, "Aircraft Icing Handbook," Vol. 2, March 1991.

[4]Palacios, Jose L., Gao, Huidong, Smith, Edward C., and Rose, Joseph L., The Pennsylvania State University,"Ultrasonic Shear Wave Anti-Icing System for Helicopter Rotor Blades," *The 62nd American Helicopter Society Annual Forum*, Pheonix, AZ, May 2006.

[5]Roglin, R.L., Kondor, S., and Hanagud, S., Georgia Institute of Technology, "Adaptive Airfoils for Helicopters," AIAA-94-1764-CP, Atlanta, GA, 1994.

[6]Epps, Jeanette J. and Chopra, Inderjit, University of Maryland, "In-Flight Tracking of Helicopter Rotor Blades Using Shape Memory Alloy Actuators," *The 40th AIAA Structures, Structural Dynamics and Materials Conference and Adaptive Structures Forum*, St. Louis, MO, April 1999.

[7]Giurgiutiu, Victor and Rogers, Craig A., University of South Carolina, "Incrementally Adjustable Rotor-Blade Tracking Tab Using SMA Composites," AIAA-97-1387, Columbia, SC, 1997.

[8]Bushnell, Glenn S., Arbogast, Darin, and Ruggeri, Robert, Boeing Phantom Works,"Shape Control of a Morphing Structure (Rotor Blade) Using a Shape Memory Alloy Actuator System," *SPIE: Active and Passive Smart Structures and Integrated Systems*, Proc. of Vol. 6928, 2008, pp. 2A1-2A11.

[9]Park, Jae-Sang, Kim, Seong-Hwan, and Jung, Sung Nam, "Application of Shape Memory Alloy Hybrid Composites for Variable-Twist Proportors," Konkuk University, *The 66th AHS Annual Forum*, Pheonix, AZ, May 2010.

[10]Prahlad, Harsha and Chopra, Inderjit, University of Maryland, "Characterization of SMA Torsional Actuators for Active Twist of Tilt Rotor Blades," *The 10th AIAA/ASME/AHS Adaptive Structures Conference*, Denver, CO, 2002.

[11]Atulasimha, Jayasimha and Chopra, Inderjit, "Behavior of Torsional Shape Memory Alloy Actuators," University of Maryland, *The 44th AIAA/ASME/ASCE/AHS Structures, Structural Dynamics, and Materials Conference*, Norfolk, VA, Apr. 2003.

[12]Geradi, J.J., Ingram, R.B., and Catarella, R.A., Innovative Dynamics, "A Shape Memory Alloy Based De-Icing System for Aircraft," *The 33rd Aerospace Sciences Meeting and Exhibit*, Reno, NV, January 1995.

[13]Geradi, Joseph J., and Ingram, Richard B., Innovative Dynamics, Inc., Ithaca, NY, U.S. Patent Application for a "Shape Memory Alloy De-Icing Technology," Patent No. 5,686,003, filed 11 Nov. 1997.

[14]Chopra, Inderjit, University of Maryland, "Review of State of Art or Smart Structures and Integrated Systems," *AIAA Journal*, Vol. 40, No. 11, Nov. 2002, pp. 2145-2187.

[15]Lagoudas, Dimitris, Hartl, Darren, Chemisky, Yves, Machado, Luciano, and Popov, Peter, "Constitutive Model for the Numerical Analysis of Phase Transformation in Polycrystalline Shape Memory Alloys," *International Journal of Plasticity*, Vol. 32-33, May 2012, pp. 155-183.